An integrated fixation and stimulus channel for adaptive optics ophthalmoscopy with a large working distance, steering field, dioptric range, and light efficiency

Yan Liu*, Marcel T. Bernucci*, Qiuzhi Ji, James A. Crowell, Kristen Bowles-Johnson,
Matthew J. Keller, Donald T. Miller
School of Optometry, Indiana University, Bloomington, Indiana
*These authors contributed equally to this work.

ABSTRACT

Adaptive optics (AO) ophthalmoscopes enable retinal imaging at cellular resolution. The small field of view (FOV) and high magnification of these instruments make inclusion of a fixation channel critical for controlling the patch of retina that is stimulated with light and imaged. Here, we develop a more powerful fixation channel that is integrated with an improved stimulus channel in the Indiana AO optical coherence tomography (AO-OCT) system. It uses all stock components except one 3D printed optical mount and some machined adaptor plates. We balanced the trade-offs between subject working distance, steering field of view, dioptric correction range, and stimulus light efficiency and achieved better performance in all areas compared to our previous channel. We report on the overarching objectives of the integrated fixation and stimulus channel, its design and its validation as illustrated by several AO-OCT imaging examples. While intended for our AO-OCT system, the design, components, and performance trade-offs are general enough to be applicable to many other AO ophthalmoscopes in the field.

Keywords: Adaptive optics, Adaptive optics ophthalmoscopy, Retinal imaging, Fixation channel, Stimulus channel

INTRODUCTION

Adaptive optics (AO) ophthalmoscopy measures and corrects ocular wavefront aberrations, enabling cellular-resolution retinal imaging and stimulation. Like microscopes, the inherently small field of view (FOV) and high magnification of these instruments make them highly sensitive to the subject's direction of gaze and ability to fixate. Most AO ophthalmoscopes therefore have an additional optics channel with a visible, controllable target that is fixated by the subject to control which patch of retina is imaged. Perhaps because of its simplistic role, the fixation channel is arguably the least reported component of AO ophthalmoscopic systems, with few details given in the literature and only one publication that we know of devoted to this topic [1]. However, this channel is challenging to develop because its design must conform to the requirements of the AO imaging and visible stimulus channels.

It is in this context that we developed a more powerful fixation channel for the Indiana AO-OCT system. The new channel integrates with a visible stimulus channel and combines with the AO-OCT beam in front of the eye. We balanced the trade-offs between subject working distance, steering field, dioptric correction range, and stimulus light efficiency and achieved better performance in all areas compared to our previous channel. Other than one 3D printed conic optical mount and some machined aluminum adaptor plates, we opted for stock components to reduce cost and lead time. While intended for AO-OCT, the design, components, and performance trade-offs are general enough to be applicable to many other AO ophthalmoscopes in the field. Here, we report on the objectives of the integrated fixation and stimulus channel, its design and its validation as illustrated by several AO-OCT retinal imaging examples.

METHODS

Several overarching objectives guided the design of the fixation and stimulus channel. Firstly, we wanted the steering FOV of the fixation target to extend beyond the nasal rim of the optic disc (>18° retinal eccentricity), covering the fundus area

Ophthalmic Technologies XXXIV, edited by Daniel X. Hammer, Kostadinka Bizheva,
Georg Schuele, Proc. of SPIE Vol. 12824, 1282402 · © 2024 SPIE
1605-7422 · doi: 10.1117/12.3003262

most critical for monitoring disease. Secondly, we wanted a working distance between subject and our ophthalmoscope to be several centimeters (i.e., long eye relief) to accommodate different head shapes (e.g., deep-set eyes) and thick facial hair. Thirdly, we needed the channel to correct 20 D range of spherical refractive errors to cover the vast majority of the population. Correcting the subject's refractive error ensures a sharp fixation target, which enhances the precision of fixation and reduces repeatability errors in longitudinal studies. Finally, to properly study retinal function, we needed accurate control of the stimulus intensity, flash duration and wavelength; the last required several orders of magnitude of background light suppression. We also needed sufficient illuminance on the retina, necessitating low light loss in the stimulus channel.

The integrated fixation and stimulus channel that we developed meets these objectives (Fig. 1). The fixation channel starts with an organic light-emitting diode (OLED) microdisplay (DSVGA150 White, eMagin) [2] that presents a white, computer-controlled, fixation target (a cross) that is imaged onto the retina by a cascade of two relay telescopes, the latter of which uses the eye's optics as the last element. The display has 800 × 600 pixels with a pixel pitch of 15 µm (nominally 17.5 µm at retina). The high brightness of the display (900 cd/m^2 (typical) and 2000 cd/m^2 (maximum)) enables us to combine stimulus and fixation channels with a 10:90 (T:R) beamsplitter, thus increasing light throughput efficiency by almost 2× compared with a 50:50 beamsplitter while maintaining an adequately bright fixation target. A camera lens (L1, Canon EFL 50mm f/1.4 7-element USM lens) conjugates the fixation target to infinity. Then, a telescope made of an objective (L2) and an eyepiece (L3) images the fixation target at infinity to the eye. L2 is composed of two 2″ diameter inverted doublet lenses (ACT508-500-A, Thorlabs); L3 is an aspheric singlet lens (BIO 14 D, Volk, EFL = 71.4 mm, diameter = 52 mm) that provides long eye relief. L3 appears to be in the wrong orientation but we found this orientation to provide better image quality as confirmed by experiments and Zemax simulation. The subject's refractive error is corrected using a Badal design realized by a motorized translation stage (Fig. 1, magenta box). L3 is the corresponding Badal lens, ideally positioned with its focal point at the nodal point of the subject's eye; this ensures that the angular location of the fixation target on the retina remains fixed regardless of the axial length of the eye. In practice, the L3 focal point is positioned slightly anteriorly to the entrance pupil of the eye [3, 4], as the location of the entrance pupil is readily determined using a pupil camera and lies close enough to the nodal point to be insensitive to the eye's axial length.

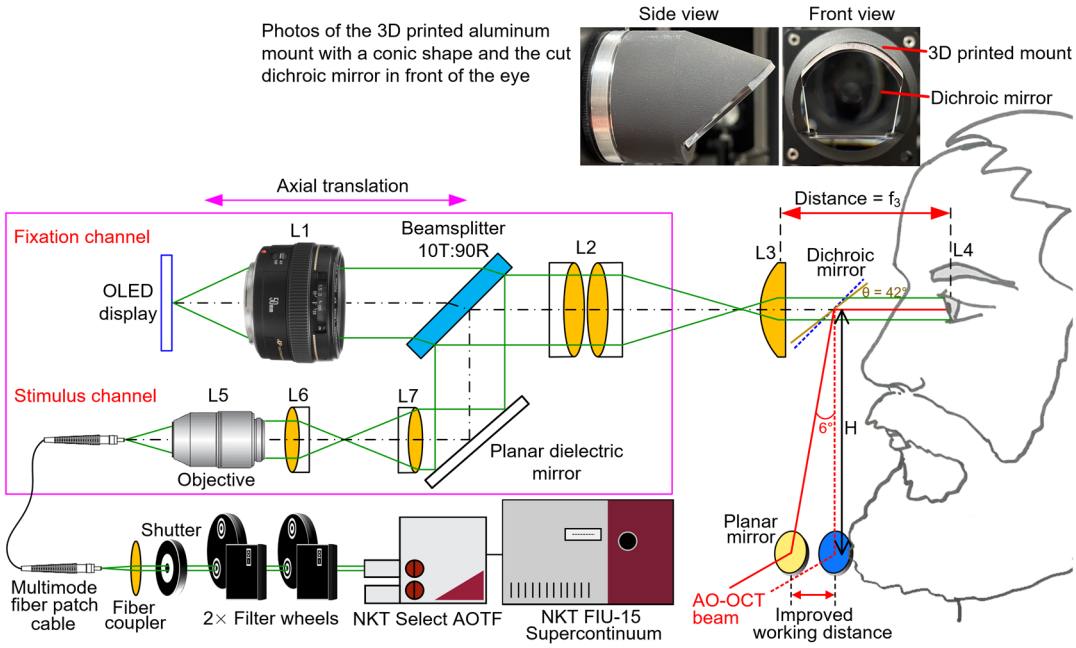

Fig. 1 Schematic of the setup for the integrated fixation and stimulation channel for AO ophthalmoscopy. H = 12 cm. L, lens; T, Transmittance; R, reflectance. Components in the magenta box are mounted on a motorized translation stage with a 4" travel range, providing a sphere correction range of 20 D. See text for description.

We determined the necessary travel range of the motorized stage to correct for 20 D range of spherical refractive errors. Using the Newtonian form of the lens equation, we find that the shift (x) of the second focal point of L2 relative to the first

focal point of L3 in order to apply a vergence P on the eye to be $x = f_3^2 P$, where f_3 is the focal length of L3. Hence, to correct for a range of refractive error, ΔP, we need to translate the stage by $\Delta x = f_3^2 \Delta P$. This equation shows that the required travel range of the stage is proportional to f_3^2, while f_3 is proportional to the working distance between the subject and our system. Therefore, a large working distance requires a long travel range of the stage, which increases system size and cost. We achieve the necessary 20 D correction range using a travel range of 4" and 14 D for L3 (i.e. f_3 = 71.4 mm).

There is another trade-off between working distance and field of view of the fixation channel. An off-axis point on the fixation display is mapped to an angle at the eye. Hence, the maximum angle that L3 subtends to the eye determines the FOV of the fixation channel. To maximize FOV, we need to maximize this angle by using a large diameter lens for L3 and placing L3 close to the eye, the latter reduces the working distance. Moreover, a dichroic mirror needs to be placed between L3 and the eye to combine with the AO imaging beam and this limits how close L3 can be placed to the eye and hence the FOV of the fixation channel.

The stimulus channel contains a supercontinuum laser (FIU-15, NKT Photonics) whose output is spectrally and temporally controlled by an acousto-optic tunable filter (AOTF; NKT Select, VIS 1×, 430-670 nm, >10 dB sidelobe suppression). Because the AOTF output contains sidelobes and other background light that can stimulate photoreceptors, we use two cascaded spectral filters from Alluxa and Semrock to further reduce this background light by 60 dB and achieve a narrow full-width at half maximum (FWHM) bandwidth of ~1.8 nm at each wavelength. We use a mechanical shutter to block the small amount of leakage light during subject alignment by opening only during the 5-ms stimulus interval. The light is then coupled into a multi-mode patch cable (Thorlabs, FG365UEC, core size = 365 µm, numerical aperture (NA) = 0.22) that disperses it and distributes it over the fiber core exit. The fiber core is imaged onto a 2° patch of retina by three pairs of relay telescope lenses, with the eye optics being the last lens.

The NA of the multimode fiber was chosen by considering the Lagrange invariant (LI), which is the product of ynu, where y is the object height, n is the refractive index and u is the ray angle. Lagrange invariant is conserved through the optical system. In our case, the fiber core is imaged onto the retina and we treat the optics in between as a black box. The Lagrange invariant at the fiber exit facet is $LI_{fiber} = ynu = (D_{core}/2) \times 1 \times NA$, where D_{core} is the fiber diameter determined from the magnification of the stimulus channel. The maximum Lagrange invariant of the eye (assuming a 6.7 mm pupil) is calculated to be $LI_{eye\_max} = y'n'u' = 0.06$ mm·rad, where $y' = 300$ µm (2° diameter retinal patch), $n' = 1.333$, $u' = D_{eye}/2/f'_{eye}$, D_{eye} = 6.7 mm, f'_{eye} = 22.22 mm. The Lagrange invariant at the fiber exit facet should be smaller than the maximum Lagrange invariant of the eye in order to minimize light loss to the 2° diameter retinal patch. This determines the maximum fiber NA to be 0.33. The fiber NA should not be too small either, because otherwise the beam size on the eye pupil becomes very small and the stimulus efficiency (coupling efficiency to photoreceptors) would be sensitive to eye alignment (i.e. lateral displacement to the stimulus beam) due to the Stiles-Crawford effect.

A dichroic mirror (DMSP680B, Thorlabs) with low loss, low wavefront error, and low group delay dispersion combines our AO-OCT, fixation, and stimulus beams. It was cut along a parabolic curve and mounted on a 3D-printed aluminum conic holder to increase the working distance by minimizing possible contact with the subject's face (Fig. 1 top row). The dichroic mirror was tilted at 42° instead of the conventional 45°, resulting in a slight tilt of the incident AO-OCT beam by 6° and thus increasing the working distance between the subject's chin and the lower mirror that redirects the AO-OCT beam upwards by 13 mm (Fig. 1).

We empirically determined the FOV of our fixation channel by first measuring the relationship between visual angle and fixation target size on two subjects (S1 and S2) with eyes of different axial lengths (25.24 mm (−3 D refractive error) and 24.14 mm (0 D refractive error)). Visual angle was determined using the calibrated galvo scanners. Then, we moved the fixation target to the edge of the subjects' FOV and recorded the location beyond which they could no longer see the target. Finally, we acquired AO-OCT images at the fixation's FOV edge to test the system's capabilities for imaging at large eccentricities. The Indiana AO-OCT is a point-scanning system that acquires A-scans at a rate of 1 MHz [5, 6]. The AO loop rate was 233 Hz with a loop gain of 1 [7].

RESULTS

The 4″ travel range of the motorized translation stage permitted refractive error correction over a 20 D range. The subject's eye was separated from the top edge and center of the dichroic mirror by 30 mm and 45 mm, respectively, as shown in

Fig. 2. We have found this working distance to be sufficient for all subjects we have imaged to date (n > 25), including those with deep-set eyes and facial hair.

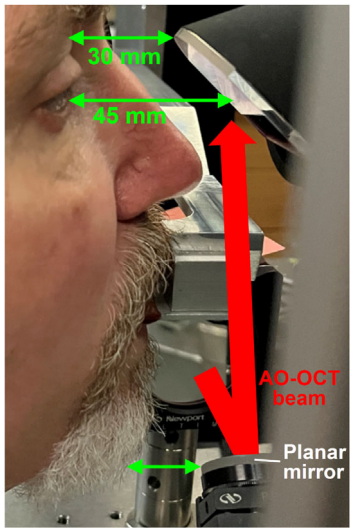

Fig. 2 Subject in the Indiana AO-OCT system. The long working distance provides adequate separation of the subject's eye from the dichroic mirror and beard from the planar mirror.

The FOV calibration conducted on the two subject eyes yielded 16 pixels/degree on the fixation display and was independent of eye axial length, as expected from the Badal principle. The steering FOV of the fixation target was determined to be 40° horizontally and 37.5° vertically (red oval in Fig. 3A), extending well beyond the optic disc and vascular arcades. Figure 3B–D show images of photoreceptor outer segments, retinal pigment epithelium cells and retinal ganglion cells at the 20° FOV edge of the fixation channel.

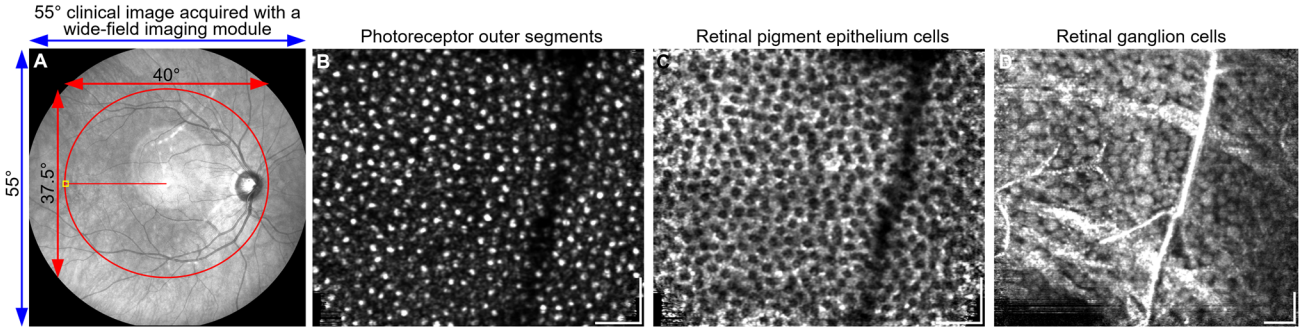

Fig. 3 Imaging the retina at 20° temporal to the fovea of a normal subject free of ocular disease. (A) The steering FOV of our system (red oval) is overlaid on a 55° clinical SLO image, acquired with a wide-field imaging lens/module of the Heidelberg Engineering Spectralis imaging system. Note that standard clinical SLO has a FOV of 30°. AO-OCT images of the photoreceptor outer segments (B), retinal pigment epithelium cells (C) and retinal ganglion cells (D) are shown at 20° temporal retina (labeled by the yellow box in A). Scale bars are 50 µm.

The ability to obtain cellular-level images at 20° retinal eccentricity that are of comparable image quality to those obtained much closer to the fovea substantiates the performance of the improved fixation channel [8-16].

CONCLUSION

Using stock components except for one 3D printed mount and some machined adaptor plates, we balanced the trade-offs between working distance, steering field of view, dioptric correction range, and stimulus light efficiency and achieved

better performance in all areas compared to the previous channel in the Indiana AO-OCT system. This work extends the retinal regions and subject population that can be studied by AO ophthalmoscopy. While constructed for use in our AO-OCT system, the design, components, and performance trade-offs are general enough to be applicable to many other AO ophthalmoscopes in the field. More details can be found in the recording of the associated SPIE Photonics West conference presentation.

ACKNOWLEDGEMENTS

This work was supported by the National Eye Institute grants R01-EY018339 and R01-EY029808. We thank Physical Sciences Inc. for their conic mount design that we modified. We thank Dan Ferguson for cutting the dichroic mirror.

REFERENCES

1. S. Steven, Y. N. Sulai, S. K. Cheong, J. Bentley, and A. Dubra, "Long eye relief fundus camera and fixation target with partial correction of ocular longitudinal chromatic aberration," Biomed. Opt. Express **9**, 6017-6037 (2018).
2. Z. Liu, F. Zhang, K. Zucca, A. Agrawal, and D. X. Hammer, "Ultrahigh-speed multimodal adaptive optics system for microscopic structural and functional imaging of the human retina," Biomed. Opt. Express **13**, 5860-5878 (2022).
3. D. Atchison, *Optics of the human eye* (CRC Press, 2023).
4. D. A. Atchison and G. Smith, *The Eye and Visual Optical Instruments* (Cambridge University Press, Cambridge, 1997).
5. O. P. Kocaoglu, T. L. Turner, Z. Liu, and D. T. Miller, "Adaptive optics optical coherence tomography at 1 MHz," Biomed. Opt. Express **5**, 4186-4200 (2014).
6. Z. Liu, O. P. Kocaoglu, and D. T. Miller, "In-the-plane design of an off-axis ophthalmic adaptive optics system using toroidal mirrors," Biomed. Opt. Express **4**, 3007-3030 (2013).
7. Y. Liu, J. Crowell, K. Kurokawa, M. Bernucci, Q. Ji, A. Lassoued, H. W. Jung, and D. Miller, *Low-latency, photon-efficient wavefront sensing for ultrafast adaptive optics imaging of the human retina*, in Ophthalmic Technologies XXXIII (SPIE, 2023), Vol. 12360, pp. 56–63.
8. Z. Liu, O. P. Kocaoglu, and D. T. Miller, "3D Imaging of Retinal Pigment Epithelial Cells in the Living Human Retina," Invest. Ophthalmol. Vis. Sci. **57**, OCT533-OCT543 (2016).
9. Z. Liu, K. Kurokawa, F. Zhang, J. J. Lee, and D. T. Miller, "Imaging and quantifying ganglion cells and other transparent neurons in the living human retina," Proceedings of the National Academy of Sciences **114**, 12803-12808 (2017).
10. E. M. Wells-Gray, S. Choi, R. Zawadzki, S. Finn, C. Greiner, J. Werner, and N. Doble, "Volumetric imaging of rod and cone photoreceptor structure with a combined adaptive optics-optical coherence tomography-scanning laser ophthalmoscope," J. Biomed. Opt. **23**, 036003 (2018).
11. E. M. Wells-Gray, S. S. Choi, M. Slabaugh, P. Weber, and N. Doble, "Inner Retinal Changes in Primary Open-Angle Glaucoma Revealed Through Adaptive Optics-Optical Coherence Tomography," J. Glaucoma **27**(2018).
12. A. J. Bower, T. Liu, N. Aguilera, J. Li, J. Liu, R. Lu, J. P. Giannini, L. A. Huryn, A. Dubra, Z. Liu, D. X. Hammer, and J. Tam, "Integrating adaptive optics-SLO and OCT for multimodal visualization of the human retinal pigment epithelial mosaic," Biomed. Opt. Express **12**, 1449-1466 (2021).
13. V. P. Pandiyan, X. Jiang, J. A. Kuchenbecker, and R. Sabesan, "Reflective mirror-based line-scan adaptive optics OCT for imaging retinal structure and function," Biomed. Opt. Express **12**, 5865-5880 (2021).
14. Z. Liu, J. Tam, O. Saeedi, and D. Hammer, "Trans-retinal cellular imaging with multimodal adaptive optics," Biomed. Opt. Express **9**, 4246-4262 (2018).
15. M. Azimipour, J. V. Migacz, R. J. Zawadzki, J. S. Werner, and R. S. Jonnal, "Functional retinal imaging using adaptive optics swept-source OCT at 1.6 MHz," Optica **6**, 300-303 (2019).
16. M. F. Shirazi, E. Brunner, M. Laslandes, A. Pollreisz, C. K. Hitzenberger, and M. Pircher, "Visualizing human photoreceptor and retinal pigment epithelium cell mosaics in a single volume scan over an extended field of view with adaptive optics optical coherence tomography," Biomed. Opt. Express **11**, 4520-4535 (2020).